CREEP AND FRACTURE OF INCONEL MA 754 AT ELEVATED TEMPERATURES

J. J. Stephens and W. D. Nix

Department of Materials Science and Engineering
Stanford University, Stanford, California 94305

Summary

The high temperature longitudinal creep and fracture properties of the mechanically alloyed oxide dispersion strengthened alloy Inconel MA 754 have been examined. Two distinct regions of deformation have been observed: a high stress, high stress exponent regime wherein plastic flow is homogeneous and fracture is transgranular, and a low stress, low stress exponent regime wherein cavitation occurs and fracture is intergranular. The cavitated transverse grain boundaries have been examined in an effort to understand the mechanism of intergranular fracture of MA 754 .

Introduction

The mechanical alloying process and refinements in thermomechanical processing have allowed the development of oxide dispersion strengthened (ODS) alloys with compositions tailored to particular high temperature applications. The most successful application of a mechanically alloyed ODS alloy to date has been Inconel MA 754 . This alloy is a nickel based alloy with yttria dispersoids and is designed for optimal creep resistance at temperatures above 1000°C. MA 754 is currently being used as a turbine vane alloy in advanced gas turbine engines (1). The creep and fracture behavior of MA 754 at temperatures of 1000°C and above have been investigated in order to understand the specific deformation processes operating at these temperatures.

Experimental Results

Materials Characterization. MA 754 is an ODS alloy with a nichrome matrix and inert refractory oxides to pin the motion of dislocations at high temperatures. The chemical composition of the heat studied in this investigation (Heat #DTO6A7B) is 76.95 Ni, 20.05 Cr, 1.32 Fe, 0.59 Y_2O_3, 0.42 Ti, 0.33 Al, 0.33 Oxygen, 0.06 C and 0.002 S , all in wt%. MA 754 requires extensive thermomechanical processing in order to achieve a highly elongated grain structure, which is essential for creep resistance. The mechanically alloyed powder is canned, extruded at an elevated temperature, and then hot worked. A subsequent 2-hour anneal at 1315°C allows for growth of highly elongated grains. This annealing procedure produces coarse grains with a low dislocation density and a relatively large number of recrystallization twins.

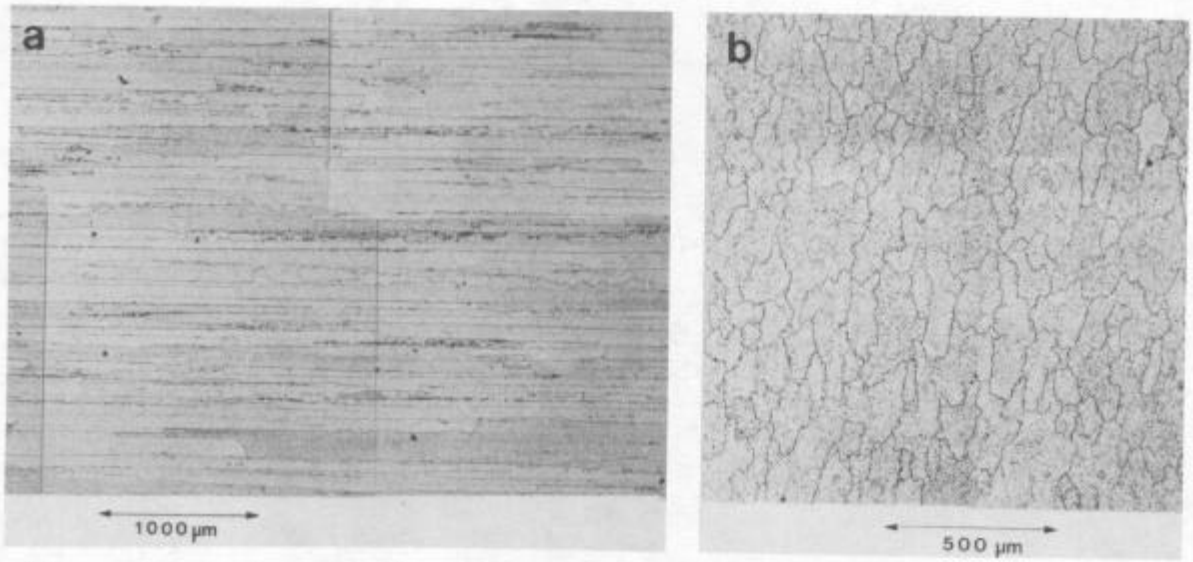

Figure 1. Grain morphology of MA 754 (Heat #DT06A7B). a) Extrusion plane, Longitudinal direction is horizontal, Long Transverse is vertical. b) Transverse plane, Short Transverse is horizontal, Long Transverse is vertical.

The grain morphology of the MA 754 heat studied is shown in Figure 1. Examination of the extrusion plane, Figure 1(a), shows the grains to be fiber-shaped, of reasonably uniform size, with relatively straight longitudinal and transverse grain boundaries. The transverse plane view, Figure 1(b), shows that a uniform fiber grain shape and size has been achieved. The virtual absence of small, included grains in this heat indicates a uniform dispersion of oxide particles, thus permitting uniform recrystallization and complete grain growth. Average intercept distances measured in the longitudinal, long transverse and short transverse directions are 714, 131 and 75 µm, respectively. These dimensions yield a grain aspect ratio of 7.2

A second important consequence of the extensive thermomechanical processing of MA 754 is the development of a strong {110}<001> texture. This texture, known as "cube on edge" is commonly encountered in fcc metals after hot working.

The pole figures of this heat are shown in Figure 2. Figure 2(a) identifies the longitudinal direction as <001>, while Figure 2(c) identifies the transverse directions as <110>. The strength of the texture is apparent from Figure 2(d), where all the (200) intensity falls within 6 degrees of the extrusion direction. Similarly, in the case of the extrusion plane, all the (220) intensity in Figure 2(b) lies within 14 degrees of the short transverse direction. This strong texture is consistent with selected area diffraction patterns, where typical grain boundary misorientations range from 4 to 8 degrees.

The resulting dispersoid morphology in MA 754 consists of mixed yttrium-aluminum oxides ranging in size from 30 to 1000 Å, occupying a volume fraction in the range 1.3-1.5%. The mean dispersoid diameter for this heat is 144 Å, as determined by transmission electron microscopy, and the particle size distribution is well approximated by a log-normal distribution. The interested reader is referred elsewhere (2) for a discussion of dispersoid size distributions in MA 754. In addition to dispersoids, MA 754 also contains relatively large inclusions with diameters as large as

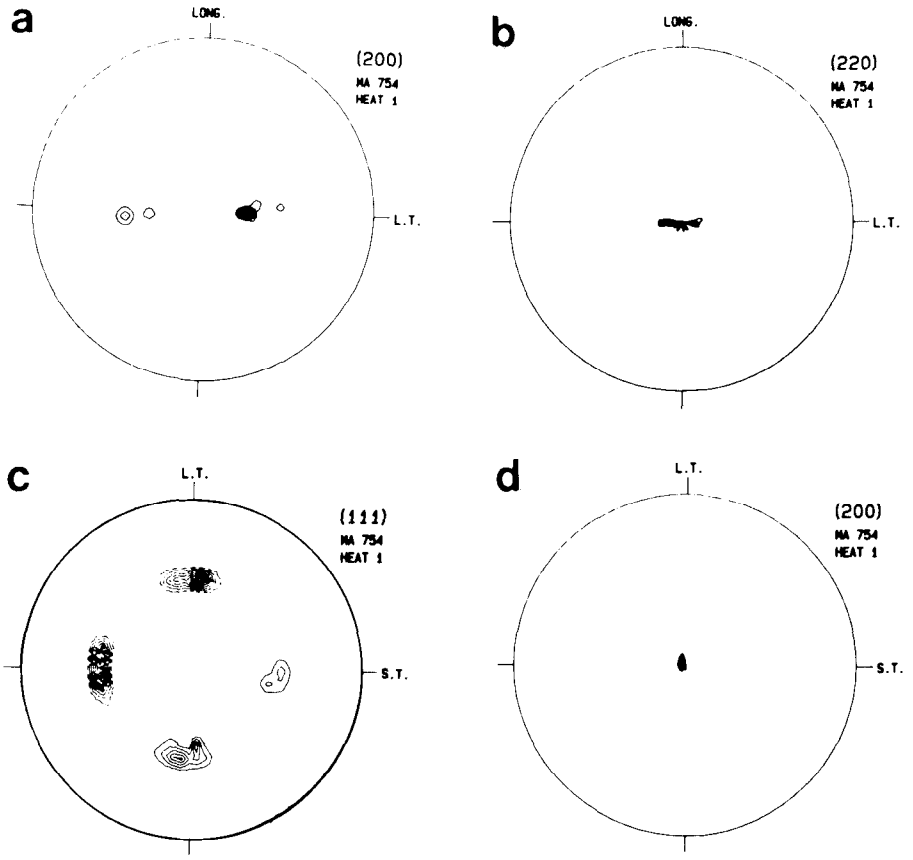

Figure 2. Pole figures of MA 754 (Heat #DT06A7B) generated in reflection. a) Extrusion plane, (200) intensity. b) Extrusion plane, (220). c) Transverse plane, (111). d) Transverse plane, (200).

1 μm. These inclusions have been identified as aluminum oxides, mixed yttrium-aluminum oxides and titanium carbonitrides (3). While these large inclusions play little or no role in pinning dislocations, their role as nucleation sites for grain boundary cavities must be considered.

Specimen Preparation and Testing Procedures. Flat specimens of MA 754 in the annealed condition were machined with the extrusion plane as the specimen flat and the stress axis parallel to the longitudinal direction. The specimen gage length was 20.3 mm. All specimens were polished to 600 grit SiC paper, and electropolished to remove surface scratches using a 30% Nital solution.

All creep testing was performed under constant stress conditions utilizing an Andrade arm in a vacuum of 10^{-5} Torr. A Type B thermocouple attached to the specimen permitted control of the test temperature to within 1°C in a 24 hour period. A tantalum extensometer utilizing a tube and rod design was employed in longer creep tests so that strain rates less than 10^{-7} (sec^{-1}) could be measured with accuracy. This extensometer was attached to a high gain (40 Volts/inch) LVDT, permitting strain resolution of 10 microstrain. The system performance allowed minimum strain rates as low as $9x10^{-10}$ (sec^{-1}) to be measured without the necessity of temperature correcting the displacement data.

Experimental Results

Creep and Fracture Data. A composite plot of minimum strain rate as a

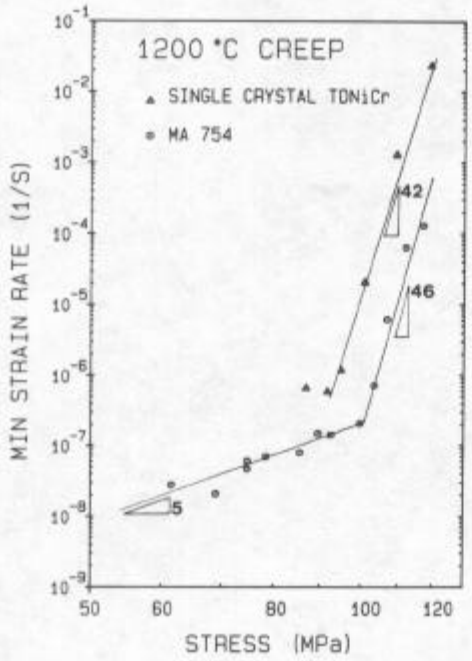

Figure 3. Constant stress creep behavior of MA 754 at 1200°C. Single crystal TDNiCr data of Lund and Nix (4) is shown for comparison.

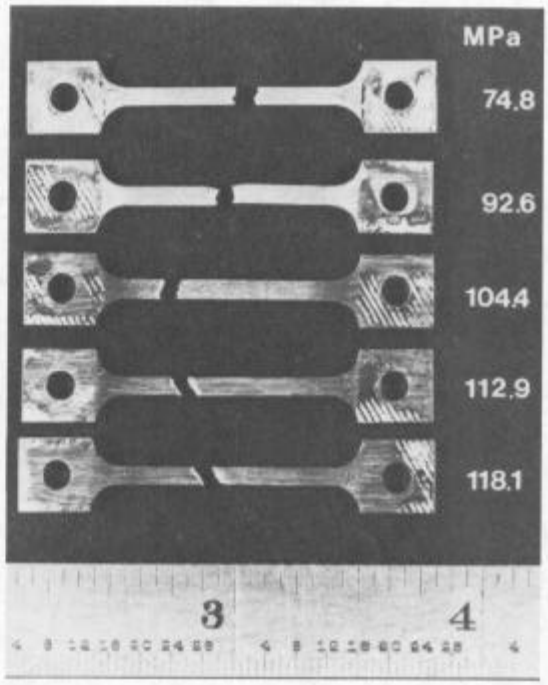

Figure 4. Fracture appearance of MA 754 specimens crept to failure at 1200°C. Applied stress is indicated to the right of each specimen. Note the transition from slanted to square fracture as the applied stress is decreased.

function of applied stress at 1200°C is shown in Figure 3. The creep data indicates there are two distinct regimes of deformation. At applied stresses greater than 104 MPa, a stress exponent, n, of 46 is observed; while at lower stresses an n value of 5 is found. This abrupt change in stress exponent is accompanied by a pronounced change in the overall fracture appearance of the specimens. Figure 4 shows the change in fracture appearance as the stress is increased. At low stresses a square fracture is observed whereas at high stresses, above 104 MPa, a slanted fracture is found. SEM examination of the fracture surfaces at low stresses indicates an intergranular fracture mode, where rupture occurs by grains pulling apart. Optical microscopy reveals cavitation of the transverse grain boundaries. Conversely, at higher stresses transgranular fracture is observed, with rupture occurring by shear across the grains.

The product of the minimum strain rate and rupture time - the Monkman-Grant constant, C_{M-G} is found to be about 2×10^{-2} at the highest stresses, and declines to 7×10^{-3} at the lowest stresses. Such a decline in C_{M-G} is to expected in light of the observed transition from transgranular to intergranular fracture.

The composite plot of minimum strain rate as a function of applied stress at 1093°C is shown in Figure 5. Again, two distinct deformation regimes are found. At stresses above 120 MPa, a stress exponent of 42 is observed, while at lower stresses n declines to a value of 16. The n value measured at low stresses is much higher than the value at 1200°C apparently because cavitation is more sluggish at 1093°C. As at 1200°C, a distinct

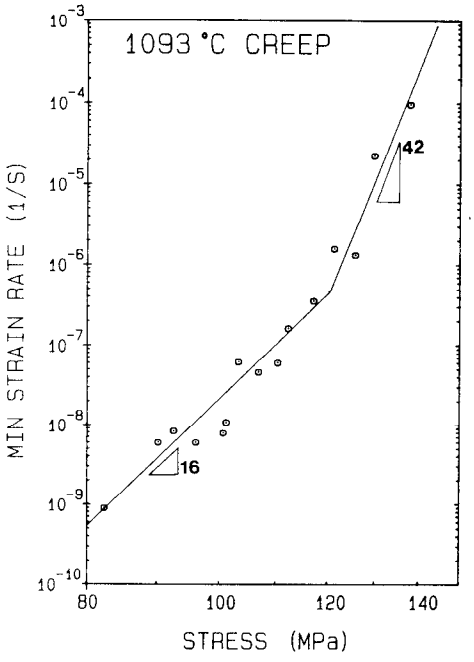

Figure 5. Constant stress creep behavior of MA 754 at 1093°C.

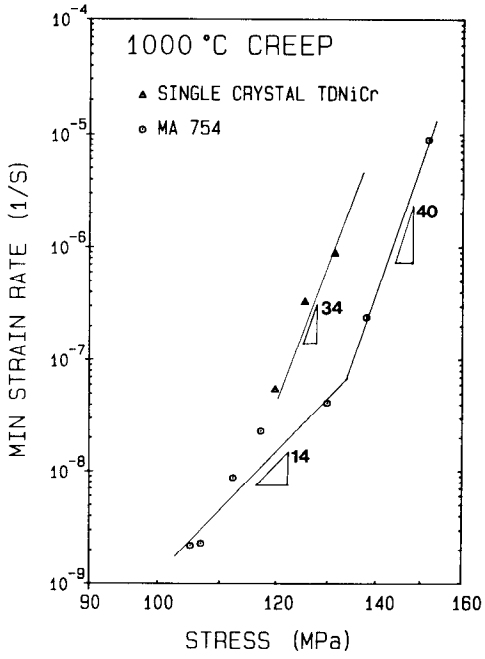

Figure 6. Constant stress creep behavior of MA 754 at 1000°C. Single crystal data of Lund and Nix (4) is shown for comparison.

transition in the overall fracture appearance is observed: slant fracture is found at high stresses whereas square fracture is observed at the lower stresses. Cavitation of transverse grain boundaries is observed in specimens crept at the lower stresses. A marked change in C_{M-G} with decreasing stress is also encountered at 1093°C: at the highest applied stresses C is 3.7×10^{-2} and it falls to 5.4×10^{-3} at the lowest stresses where rupture occurred.

The creep response at 1000°C is very similar to behavior observed at 1093°C. The composite plot of minimum strain rate as a function of applied stress at 1000°C is shown in Figure 6. The high stress n is 40, whereas at stresses below 133 MPa n declines to 14. Cavitation of the transverse grain boundaries is observed at the lower stresses.

Examination of Cavitated Transverse Grain Boundaries. As discussed above, optical metallography indicates that cavitation of the transverse grain boundaries occurs for specimens crept at the lowest stresses. The extent of cavitation in a ruptured specimen is most extensive at stresses slightly less than the 'crossover' stress, i.e, the stress above which creep is homogeneous. An example of this maximum cavitation is shown in Figure 7 for a specimen crept at 1093°C to failure in 23.8 hrs at 113.3 MPa. Figure 7(a) shows the overall cavitation at a position on the gage length approximately four to five grain lengths away from the fracture surface. Note that there is a variation in the extent of cavitation of the transverse grain boundaries.

An electron microprobe analyser with a beam width of 1 μm was used in a spot analysis mode to determine if dispersoid-free zones are formed during the course of creep. It is found that yttrium signals are lower than the bulk only in the immediate vicinity of transverse grain boundary cavities.

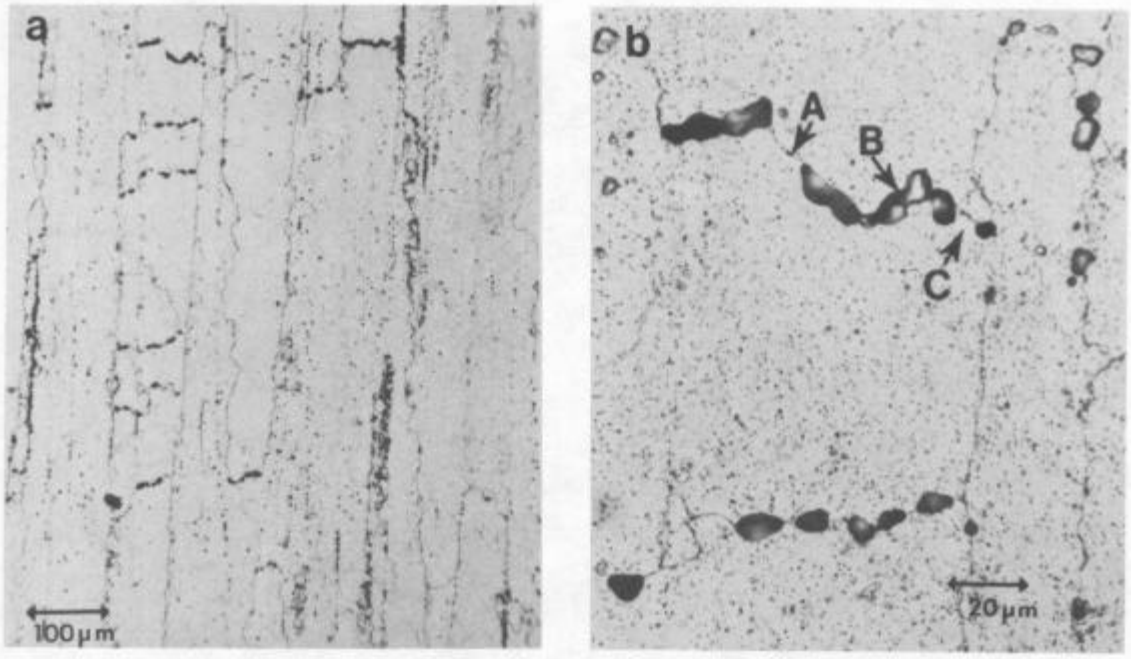

Figure 7. Cavitation behavior of a MA 754 specimen crept to failure in 23.8 hrs at 1093°C, 113.3 MPa. Applied stress axis is vertical. a) Overall view of cavitated grain boundaries. b) Closeup of upper left quadrant of A. Points A,B,C indicate location of microprobe spot analyses for yttrium, where Y_2O_3 levels of 0.30, 0.02 and 0.03 wt%, respectively. were measured.

In Figure 7(b), spots B and C show Y_2O_3 contents which are 1/25 of that measured in the bulk (0.50 wt% Y_2O_3). Point A, approximately 4 µm away from a cavity, shows a yttria level approximately 1/2 of that in the bulk. Other spot analyses further removed from cavities in transverse grain boundaries yield yttrium signals equal to the bulk. These results indicate that small dispersoid free zones form adjacent to the transverse grain boundary cavities.

Additional evidence for dispersoid-free zone formation adjacent to cavities is provided by transmission electron microscopy. Figure 8 shows the region adjacent to a transverse grain boundary in a specimen crept to failure at 1093°C in 30.6 hrs, at an applied stress of 103.3 MPa. Figure 8(a) indicates the overall geometry. The region of interest lies in the vicinity of the arrow which marks the stress axis. The area in the transverse grain boundary immediately to the left of the cavity is shown in Figure 8(b). A dispersoid-free zone about 1 µm wide is found in the transverse grain boundary. Close inspection of this micrograph reveals a few small dispersoids in this region - but they are so widely spaced that easy deformation is expected in this region. Thin foil electron microscopy of uncavitated transverse grain boundaries in crept specimens show dispersoid distributions representative of the bulk material. Thus, dispersoid-free zones are found only in the immediate vicinity of transverse grain boundary cavities in MA 754 .

Discussion of Results

High Stress Regime. All three temperatures at which creep tests were performed exhibit n values of 40 and greater at the higher stresses. These n values are of the same magnitude as those found for <001> single crystal TDNiCr by Lund and Nix (4). The 1200°C and 1000°C data from that study are plotted in Figures 4 and 6, respectively. It is apparent that the high stress exponent regime for MA 754 basically represents single crystal behavior:

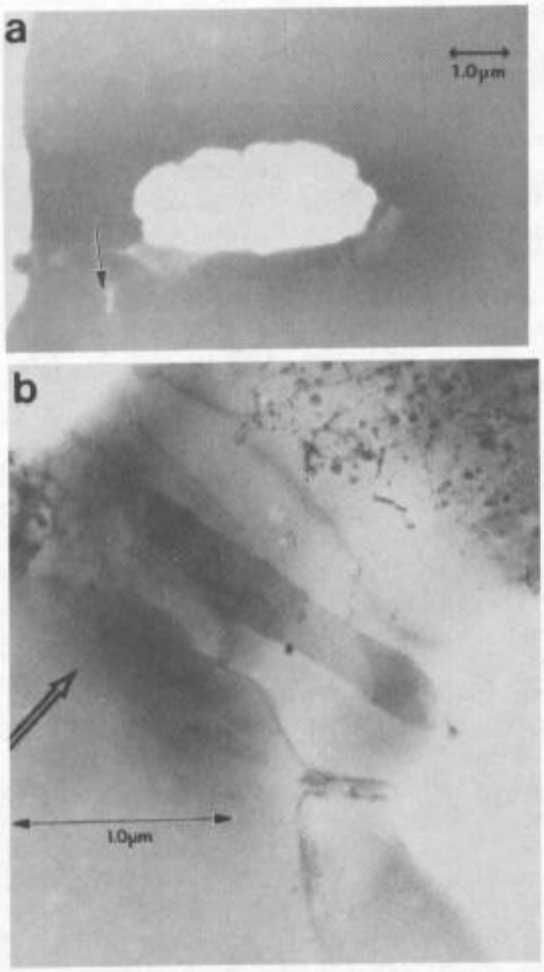

Figure 8. Transmission Electron Micrographs of area adjacent to a transverse grain boundary cavity in a specimen crept to failure in 30.6 hrs at 1093°C, 103.3 MPa. Stress axis is indicated by arrows. a) Low magnification view including cavity. b) Close-up of region in the vicinity of stress arrow in A. A dispersoid-free zone 1 μm wide is observed immediately adjacent to the cavity.

the high stresses exceed the Orowan stress and creep occurs by dislocation processes. Here, the creep process is homogeneous and fracture is transgranular. The transverse grain boundaries in MA 754 have insufficient time to cavitate at these high strain rates.

The decrease in stress exponents in MA 754 with decreasing temperature (in the high stress exponent regime) can be explained in terms of single crystal behavior. This behavior is qualitatively explained (4) by viewing the creep strength of the single crystal as the sum of the Orowan stress and the matrix strength of nichrome. As the temperature decreases, the matrix strength of nichrome with n=5 represents an increasingly larger fraction of the single crystal strength, leading to a decrease in n over the measured range of strain rates.

Low Stress Regime. As mentioned earlier, the low stress regime for MA 754 is marked by a low value of n, along with cavitation of transverse grain boundaries and subsequent intergranular fracture. Since cavitation occurs, the measured n values cannot be compared directly with n values measured for homogeneous steady-state creep. Other investigators have studied the creep properties of MA 754 in the temperature range examined here. Whittenberger (5) measured an n value of 18 for longitudinal creep in MA 754 at 1093°C. This is in reasonable agreement with the n value of 16 measured in this study. Howson, et al (3) measured n values of 33 and 27 at 982 and 1093°C, respectively. The stress exponent at 982°C was calculated from data which spans the two deformation regimes observed in this study. The 1093°C data of Howson, et al. does not extend over a strain rate range broad enough to permit accurate determination of a stress exponent. Due to the high n values characteristic of ODS alloys, it is necessary to conduct creep experiments over a broad range of strain rates in order to determine n accurately.

Cavitation Behavior. The microstructural evidence presented above for dispersoid-free zone formation near transverse grain boundary cavities implies that intergranular fracture of MA 754 occurs by means of local diffusive processes. The dispersoid-free zones apparently form by plating out metal atoms from the cavity onto the adjacent grain boundary. No evidence for continuous dispersoid-free zones in transverse grain boundaries was found.

As the transverse grain boundaries cavitate, they must shed load onto neighboring grains since the cavitated and dispersoid-free regions will not

bear any load. This load shedding leads to increased stresses in the adjoining grains, and ultimately leads to fracture. The process of intergranular fracture in MA 754 can be understood by considering how cavities can grow in the transverse grain boundary. In a coarse, elongated grain structure, the volume plated into the transverse grain boundaries spreads the two grains apart a distance u. This displacement u must be accommodated by either deformation or sliding of adjoining grains. The cavity growth is thus constrained by the rate at which these accommodating processes can occur. Constrained cavity growth in alloys was first considered by Dyson (6) and later refined by Rice (7). In a future publication (8) we will apply the constrained cavity growth model to the creep deformation behavior of MA 754 .

Conclusions

The longitudinal creep behavior of coarse-grained MA 754 at elevated temperatures consists of two major deformation regimes. At high stresses, n values of 40 and greater are observed, and fracture is transgranular. The measured n values in this regime are about the same as those for single crystal TDNiCr, and one can view this regime as single crystal behavior. At lower stresses, a second deformation regime is encountered, with low n values accompanied by cavitation and intergranular fracture. Small, dispersoid-free zones are observed immediately adjacent to the transverse grain boundary cavities. Intergranular fracture in coarse-grained MA 754 apparently results from local diffusive processes rather than bulk transport mechanisms such as Nabarro-Herring creep. The growth of transverse grain boundary cavities in coarse-grained MA 754 is constrained by the deformation of adjoining grains.

Acknowledgements

We would like to acknowledge the support of the Air Force Office of Scientific Research, through the grant AFOSR-81-0022C. We are grateful to INCO for supplying us with the material used in this investigation.

References

1. W. Crawford, "Oxide Dispersion Strengthened Materials in Advanced Gas Turbine Engines - MA 754 Vanes", J. S. Benjamin, ed.; Frontiers of High Temperature Materials II, INCO MAP, 1983.
2. J. J. Stephens and S. Spooner, "Determination of Dispersoid Size Distributions in an Oxide Dispersion Strengthened Alloy", to be submitted to Journal of Materials Science, 1984.
3. T. E. Howson, J. E. Stulga and J. K. Tien, "Creep and Stress Rupture of Oxide Dispersion Strengthened Mechanically Alloyed Inconel Alloy MA 754 ", Met. Trans., 11A, 1599 (1980).
4. R. W. Lund and W. D. Nix, "High Temperature Creep of Ni-20Cr-2ThO2 Single Crystals", Acta Metallurgica, 24, 469 (1976).
5. J. D. Whittenberger, "Creep and Tensile Properties of Several Oxide Dispersion Strengthened Nickel Base Alloys", Met. Trans., 8A, 1155 (1977).
6. B. F. Dyson, "Constraints of Diffusional Cavity Growth Rates", Metal Science, 10, 349 (1976).
7. J. R. Rice, "Constraints on the Diffusive Cavities of Isolated Grain Boundary Facets in Creeping Polycrystals", Acta Metallurgica, 29, 675 (1981).
8. J. J. Stephens and W. D. Nix, to be submitted to Met. Trans., 1984.